

# COMSOL<sup>®</sup> simulations of supersonic flow fields to study trajectories of aerosols and their impact efficiency on a rocket-borne particle collector

B. S. Klug<sup>1</sup>, A. Hundertmark<sup>1</sup>, R. Weigel<sup>2</sup>

1. Institute for Mathematics, RPTU Kaiserslautern-Landau, Landau, Germany

2. Institute for Atmospheric Physics, JGU Mainz, Mainz, Germany.

## Abstract

This investigation applies computational fluid dynamics simulations to support the design development of an impaction-based particle collector. This collector aims at submicron aerosol sampling in the supersonic free stream radially aside a sounding rocket body in the mesosphere (altitude of 85 km). The overall goal of the development process is to collect mesospheric aerosols for their physico-chemical analyses to gain further insights into high atmosphere processes: e.g. of aerosol particles from meteoric ablation and their potential impact on noctilucent cloud (NLC) formation. However, sampling of particles at these heights and their analyses is only possible by considerable costs and great effort by using sounding rockets, which is why only a sparse database is available so far. The development process and efficiency analyses are based on numerical simulations achieved by the software COMSOL Multiphysics<sup>®</sup>, where the simulation workflow is divided into two independent studies: First, with the CAD Import Module in COMSOL<sup>®</sup>, the detailed rocket geometry (as far as relevant for the particle collection efficiency) is implemented into the model. Then, the supersonic flow field surrounding the rocket under varying flight attitudes is simulated by the High Mach Number Laminar Flow Interface in COMSOL Multiphysics<sup>®</sup> by solving the Navier-Stokes equations for compressible fluids, whereby a steady state solution is obtained. Of particular interest for the design and arrangement of the probe collector is (a) the evaluation of the evolving flow field around the sounding rocket at the free stream Mach number of  $Ma = 1.75$  (at 85 km height) and (b) the localization as well as the impact of the occurring shockwave on the particle sampling. Furthermore, the thickness of the boundary layer around the rocket body is investigated to ensure a particle sampling well away of perturbing influences. Additionally, for modeling the particle trajectories and thus the aerosol impactions on the probe collector, Particle Tracing for Fluid Flow in COMSOL<sup>®</sup> is utilized, where Newton's second law is applied. For this purpose, a preliminary investigation of possible particle forces and their magnitude is performed and corresponding forces (drag and Brownian force) are considered in the model. With the final collector design, the number of impacted particles (by particle counter application in COMSOL Multiphysics<sup>®</sup>) on collector surfaces are analyzed in a parameter study (*Parametric Sweep*) for aerosol sizes of 1.2 nm diameter at various number concentrations. Therefrom, the potential sampling efficiency of the probe collector is estimated. In conclusion, impactions onto designated collector surfaces are highly probable according to simulation results. Moreover, our COMSOL<sup>®</sup> model can be validated by measurement results of the future planned rocket flight.

**Keywords:** CFD – supersonic flow regimes – particle impactions.

## Introduction

Every day, large amounts of cosmic material enter the Earth's atmosphere as the Earth moves through the dusty far reaches of our solar system. It is estimated that the quantity of incoming material ranges between 3 and 300 tons per day [1]. Most of the incoming interplanetary solids ablate as they enter the upper atmosphere by enhanced frictional heating (of more than 1800 K) from collisions of the cosmic bodies with air molecules (due to their velocities ( $> 40 \text{ km s}^{-1}$ ), sizes ( $> 10 \mu\text{m}$ ), and masses ( $> 10^{-7} \text{ g}$ ) [2]), where the cosmic bodies' temperature increases accordingly reaching the boiling point of various of the meteor's constituents. Consequently, the volatilized meteoric material (the ablation peaks at 90 km altitude [1]) is assumed to undergo rapid recombination and polymerization. This presumably leads to clusters that further agglomerate and form nanometer-sized aerosol particles, so-called meteoric smoke particles (MSP) [3] [4] [5] [6] [7] [8]. MSP are thought to have a

significant importance in the mesospheric formation of ice particles, as they can serve as ice condensation nuclei, e.g., of so-called noctilucent clouds (NLC) that occur at 85 km altitude north of  $50^\circ$  [9] [10] [11] [12] or faint layers of ice particles detected by means of back-scattered radar signals, an observational phenomenon that is denoted as polar mesospheric (summer/winter) echo [13]. So far, however, little is known about MSP and their role within the NLC formation: (a) particle samples or experimental evidence of MSP as ice condensation nuclei at the corresponding altitude is lacking so far, (b) the particle number concentrations or the size distribution of MSP are not yet comprehensively known, and (c) neither is the chemical composition or the morphology of MSP if they are involved in mesospheric cloud processes [14]. Reasons of the existing research gap in the upper atmosphere are the challenges in performing experimental measurements (i.e., taking particle samples) at such altitudes, where the collection of aerosols is only possible by means of sounding rockets. Since instrument

operation on such a measuring platform is inherent with considerable costs and is linked to a high level of effort, this investigation aims to support the design development of an inertia-based aerosol collector by using numerical simulations with COMSOL Multiphysics® (while, based on the knowledge gained, the probe collector is further developed and adapted). In addition, the performance of the particle collector is characterized. The overarching motivation of the research project is to develop a measuring device for the collection of NLC elements and constituents during a sounding rocket flight, as impacted elements on the particle collector presumably contain their ice nuclei (e.g., MSP), which then could be specified in subsequent physico-chemical analyses.

### Numerical modelling

Simulations are carried out with the COMSOL Multiphysics® [15] simulation software utilizing the Computational Fluid Dynamics (CFD) and Particle Tracing Module applying the unique ambient conditions of the mesosphere. In addition, NLC elements (particle diameters of  $< 12 \mu\text{m}$  [16] [17] [18] [11] [19]) or MSP (nanometer-sized aerosols of  $< 9 \text{ nm}$  [14] [20] [21] [22] [23] [24] [25]) are considered. In a first step, fluid dynamics simulations are performed at a Mach number of  $\text{Ma} = 1.75$  (supersonic flow conditions) at an altitude of 85 km (corresponding to a velocity of  $400 \text{ m s}^{-1}$ ). The rocket's varying attitude is taken into account by simulations conducted for different angles of attack (between  $+30^\circ$  and  $-30^\circ$ ), which occur during the (flattened ballistic) flight path (i.e., in which the rocket is kept hovering [26]). The simulations are aimed at analyzing the evolving shockwave and boundary layer thickness to determine the position, arrangement and design of the particle collector with its impactor surfaces. In a second step, the particle trajectories in the near-field of the particle collector are calculated based on simulated flow fields while taking the relevant particle forces into account, which are the Stokes' drag and the Brownian force. The effectiveness and the efficiency of the probe collector is estimated by means of our simulations based on varying particle number concentrations performed with a *Parametric Sweep*.

### Supersonic flow simulations

As a first step for the flow simulations, the detailed geometry of the instrument module of the payload (cf. *Figure 1*) is imported using the COMSOL® CAD Import Module. The rocket geometry downstream of the instrument compartment (future location of the particle collector) remains unconsidered for simulations since the flow patterns in the wake of the particle collector are irrelevant to the development process. After determining the free stream Reynolds number of  $\text{Re} < 425$ , simulations of the supersonic flow field around the instrument module are

performed utilizing the High Mach Number Laminar Flow Interface of COMSOL®, solving the Navier-Stokes equations for compressible fluids along with the energy equation, the internal energy equation, and the ideal gas law:

$$\frac{\partial \rho}{\partial t} + \nabla \cdot (\rho \vec{u}) = 0 \quad (1)$$

$$\frac{\partial(\rho \vec{u})}{\partial t} + \nabla \cdot (\rho \vec{u} \vec{u}^T) = -\nabla p \mathbf{I} + \nabla \cdot \left[ \mu \left( \nabla \vec{u} + (\nabla \vec{u})^T - \frac{2}{3} (\nabla \cdot \vec{u}) \mathbf{I} \right) \right] + \rho \vec{f} \quad (2)$$

$$\frac{\partial}{\partial t} \left[ \rho \left( e + \frac{u^2}{2} \right) \right] + \nabla \cdot \left[ \rho \vec{u} \left( e + \frac{u^2}{2} \right) \right] = -\nabla \cdot \vec{q} + Q + \nabla \cdot (\sigma \vec{u}) + \rho (\vec{f} \cdot \vec{u}) \quad (3)$$

$$e = c_v T \quad (4)$$

$$\rho = \frac{p}{R_s T}, \quad (5)$$

where  $\rho$  is the fluid density,  $\vec{u}$  is the fluid velocity,  $\mathbf{I}$  is the identity matrix,  $\mu$  the dynamic viscosity,  $\vec{f}$  the net body force per unit mass,  $e$  is the internal energy,  $\vec{q} = -k \nabla T$  the heat flow vector,  $k$  the thermal conductivity,  $Q$  represents the heat sources,  $\sigma$  is the Cauchy stress tensor,  $c_v$  the specific heat capacity, and  $R_s$  the specific gas constant (note:  $c_v$  is a temperature dependent variable but is assumed to be constant. This results in an error of less than  $\pm 1.1\%$  [27] and is therefore negligible in terms of a linear coefficient in Equation 4). Required parameters are set accordingly to the (atmospheric) conditions at the altitude of 85 km such as the gravitational acceleration of  $g = 9.5 \text{ m s}^{-2}$ , the temperature of  $T = 130 \text{ K}$  [28] [10], and the static pressure of  $p = 10^{-2} \text{ hPa}$  [10]. In our reference frame, the air flow around the stationary rocket geometry is considered, where the rocket is not moving.

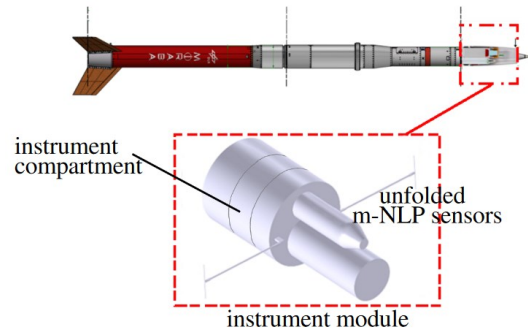


*Figure 1: Sounding rocket and the instrument module with instruments located underneath the rocket's nose cone, which is blown off prior to the measurement flight phase (based on [26]). The compartment of the instrument module housing the probe collector is referred to as the instrument compartment.*

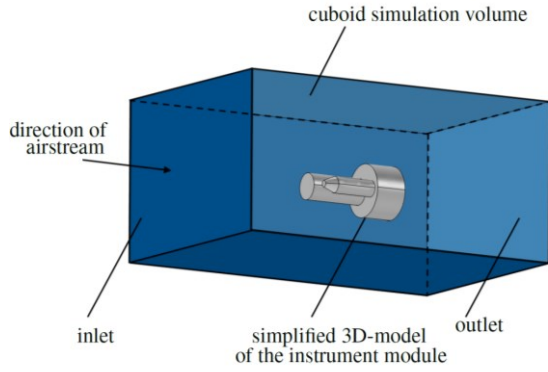


Figure 2: Schematic representation of the simulation volume, with the instrument module aligned in the flow direction and located at the center of the volume. The fluid enters the simulation volume through the inlet located upstream of the instrument module. The flow's outlet is at the rear of the simulation volume.

The schematic of the model setup is shown in Figure 2, where the flow inlet is defined upstream of the instrument module and accordingly all other outer boundaries are depicted with the (hybrid) outlet boundary condition:

$$\left( -pI + \left( \mu(\nabla\vec{u} + (\nabla\vec{u})^T) - \frac{2}{3}\mu(\nabla\vec{u})I \right) \right) \vec{n} = -0.5(p - p_{stat})\vec{n}, \quad (6)$$

if  $Ma < 1$ , where  $p_{stat} = 1$  Pa is the outlet pressure, and

$$\left( -pI + \left( \mu(\nabla\vec{u} + (\nabla\vec{u})^T) - \frac{2}{3}\mu(\nabla\vec{u})I \right) \right) \vec{n} = -pI\vec{n}, \quad (7)$$

together with following equation

$$-\vec{n} \cdot \vec{q} = 0, \quad (8)$$

if  $Ma \geq 1$ . The boundary of the instrument module is defined by the no-slip boundary condition. Finally, the fluid considered for the simulations is defined as air using the COMSOL® material library. A time-dependent study is applied for the simulations of the supersonic flow to obtain a steady-state flow field, on the basis of which analyses are performed. The user controlled computational mesh for fluid flow is shown in Figure 3 a) with smallest mesh element sizes of  $1.89 \cdot 10^{-3}$  m in the vicinity of the instrument module geometry, where eight layers of boundary elements are set up around the instrument module as shown (largest element sizes are of 0.19 m in the far field). The resulting velocity magnitudes are depicted in Figure 3 b). Clearly visible is the evolving bow shock at the instrument module tip, which interferes with further shockwave structures at the tips of the unfolded m-NLP sensors (cf. Figure 1). The boundary layer at the instrument compartment is well defined and is analyzed along the cut lines shown in Figure 4 to determine a sufficient distance between the position of the impaction surfaces and the vehicle fuselage:

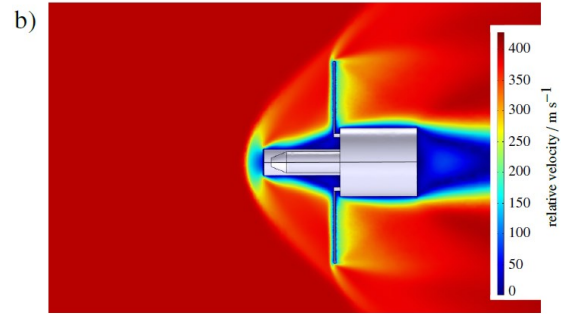
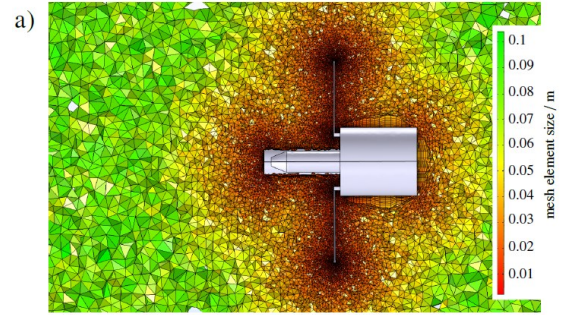


Figure 3: a) Computational mesh generated for fluid flow simulations. The mesh resolution is enhanced in the vicinity of the instrument module and boundary layer elements are created at the module's surface. b) Stationary airflow surrounding the instrument module, where the bow shock forms at the instrument module tip. Flow direction is from the left to the right.

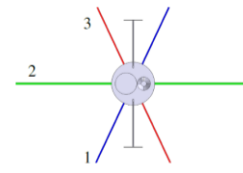


Figure 4: Instrument module with three cut lines (cut line 1: blue, cut line 2: green, and cut line 3: red) indicating the axes along which the flow velocities are analyzed.

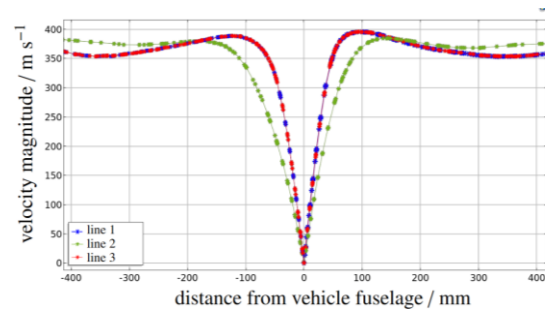
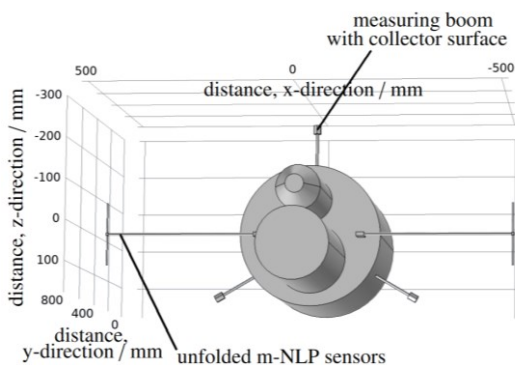


Figure 5: Flow velocities evaluated along cut lines 1 (blue), 2 (green), and 3 (red) as shown in Figure 4. Data points at mesh nodes are indicated by crosshair symbols.

Particle sampling beyond this determined distance prevents influences of the boundary layer on the collection process. The spatial angles under which the cut lines 1 (blue), 2 (green), and 3 (red) are aligned to each other and to the instrument module exclude wake effects due to upstream structures (e.g., protruding geometries, m-NLP sensors) and

represent favorable orientations for the individual booms of the particle collector. The evaluated velocity values are shown in *Figure 5* for cut lines 1, 2, and 3. The zero point of the x-axis coincides with the two cross-section points of the intersection lines with the vehicle fuselage. On profiling the velocity field along the cut lines, negative values indicate decreasing, and positive values increasing distances from the rocket body. The boundary layer is represented by the extreme drop of velocity values (see *Figure 5*). The boundary layer thickness may correspond to a distance of about 110 mm from the surface of the instrument module, such that a distance of 120 mm or more appears sufficient for particle collections largely undisturbed by the boundary layer. Noticeably, the velocity profile along cut line 2 deviates by some extent from the profiles along cut lines 1 and 3. To explain this, the course of cut lines through the simulation geometry needs to be accounted for: for cut lines 1 and 3, the geometry of the instrument module is symmetrical to the zero point, but asymmetrical for cut line 2. Other than this, no further influence of protruding geometry structures on the flow pattern at the selected cut line positions is evident from the simulations.

Finally, the position, reach, and orientation of the particle collector is determined: From the previous simulations, the radial exposure of the impaction surfaces corresponding to the cut lines is ideal - the length of the booms (as distance to the rocket fuselage) is set to 120 mm. The final instrument setup is shown in *Figure 6*: three impaction surfaces (with a non-aerodynamic shape as depicted that favors aerosol impaction) are attached to the tips of booms where the aerosols are to be hit for collection. For the following simulations of the fluid flow, the computational mesh is further refined in close proximity to the impaction surfaces (see *Figure 7*, with smallest mesh element sizes of  $1.15 \cdot 10^{-3}$  m and largest elements of 0.1 m) to adequately resolve small-scale flow pattern especially in the wake of the booms.



*Figure 6: Geometry of the instrument module as seen from the front. The three booms, which carry the substrate mounts at their tips, are arranged in an offset configuration to the m-NLP sensors.*

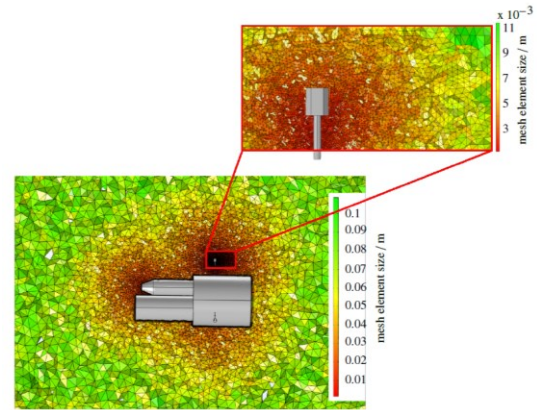


*Figure 7: Generated mesh for simulating fluid flows around the geometry of the instrument module. A high-resolution mesh, created around the collector surfaces is shown in detail for the upright boom.*

Then, the flow around the instrument module is simulated at different angles of attack of  $0^\circ$  and  $\pm 30^\circ$ . Ultimately, the simulation results confirm the boom length of 120 mm as sufficient to ensure undisturbed particle collection outside the boundary layer of the instrument module. In general, the simulation results reveal the direct or indirect exposure of the collector surfaces in the free stream, as shown in *Figure 8 a)* and *b)* for the angles of attack of  $\pm 30^\circ$ . The asymmetric shock waves are clearly visible, whereby at the flight attitude of  $+30^\circ$  only the two booms on the fuselage underside are directly exposed to the free flow, while the boom on the upper fuselage sits in the flow shadow of the instrument module (at  $-30^\circ$  and  $0^\circ$  all three booms are directly exposed).

### Simulations of particle trajectories

Particle trajectories are calculated by means of the COMSOL<sup>®</sup> Particle Tracing Module, whereby -- based on the negligible particle volume -- a one-way coupling is considered (i.e., only the flow field affects particle advection but not vice versa). Therefore, two separate but coupled time-dependent studies [29] (one for the fluid flow and one for the particle tracking) are included in our simulations, where fluid velocity values at the particle positions are required as input to determine the position and velocity of the particles at the next time step of the simulations. For the particle equation of motion, a preliminary study of possible particle forces (i.e., the Stokes' drag force, the Brownian force, the Saffman force, the gravitational force, the added mass force, and the pressure gradient force) and their magnitudes are conducted. As a result, only the Stokes' drag force and Brownian force are accounted for in the model due to their substantial effects, while all other forces were found being negligible.

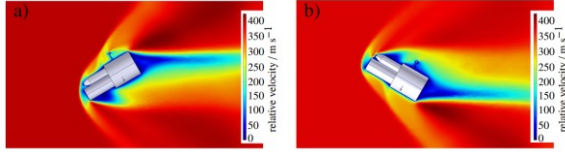


Figure 8: Stationary flow fields around the instrument module for the angles of attack of  $-30^\circ$  (shown in a), and for  $+30^\circ$  (shown in b), respectively.

The final particle equation of motion is obtained as:


$$m_p \frac{d^2 \vec{x}}{dt^2} = \vec{\zeta} \sqrt{\frac{6 \pi \mu_f k_B T d_p}{\Delta t C_c}} + \frac{3 \pi \mu_f d_p \vec{u}_r}{C_c}, \quad (9)$$

where  $m_p$  is the mass of the particles,  $\vec{x}$  is the particle position vector,  $t$  is the time,  $\vec{\zeta}$  is a vector of independent normally distributed Gaussian random numbers,  $\mu_f$  is the dynamic viscosity of the fluid,  $k_B$  the Boltzmann constant,  $T$  the temperature,  $d_p$  the particle diameter,  $\vec{u}_r$  the relative particle velocity, and  $C_c$  the Cunningham Slip corrector. Parameters applied in the particle simulations include the aerosols of smallest size, i.e. MSP, with diameters of 1.2 nm [25] and the material density of  $3 \text{ kg m}^{-3}$  [28] in the sense of an extreme value approach. A fortiori, larger particles, such as NLC elements, will impact anyway due to their greater inertia. Applied aerosol concentrations range from 1 to  $38 \text{ cm}^{-3}$ , which is the lower limit of assumed mesospheric aerosol number concentrations [9] [11] [30] [31]. For the simulations, these concentrations need to be converted to total aerosol numbers contained in the entire computational volume. With regard to the computational effort to simulate instantaneously released particles and with the aim of an efficient computation regarding the time step reduction for impacting particles controlled by the solver, the three-dimensional aerosol distribution in the fluid volume is converted into a two-dimensional plane of randomly arranged aerosols released at only two time instances. The aerosol numbers are initialized at the particle inlets from which the aerosols enter the simulation volume at their terminal velocities. A further improvement in terms of computational efficiency results from restrictions regarding the inlet positions and the size of the particle inlets into the simulation volume, from which the released aerosols impact the collector surfaces with highest probability. For this purpose, backward trajectories of the impacting particles are analyzed to determine the positions of the particle inlets. Thus, particles in the far field of the instrument module, which are irrelevant for impactations do not take up computational capacity.

### Effectiveness and efficiency of inertia-based aerosol collection

The impactation patterns of 2703 particles deposited on the collector surfaces for an aerosol number concentration of  $11 \text{ cm}^{-3}$  are shown in Figure 9. Analogous results from simulations performed with a *Parametric Sweep* of collected particles at different

number concentrations (where the number of impacted particles is determined with the particle counter evaluation provided by COMSOL®) provide further insight into the collection effectiveness of the individual impactation surfaces. For reasons of symmetry and for the sake of reducing computational effort, only one of the two downside-oriented booms is considered for simulating the particle impactation onto respective collection surfaces.

 direction of flow

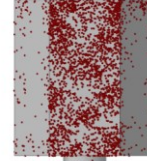


Figure 9: 2703 particles impactation pattern onto a collector surface at an initial aerosol number concentration of  $11 \text{ cm}^{-3}$ .

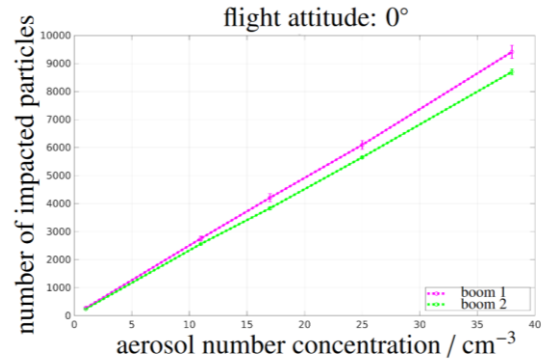


Figure 10: Number of collected particles related to initial aerosol number concentrations for the angle of attack of  $0^\circ$ . Vertical bars represent the random impactation dispersion of four independent model runs.

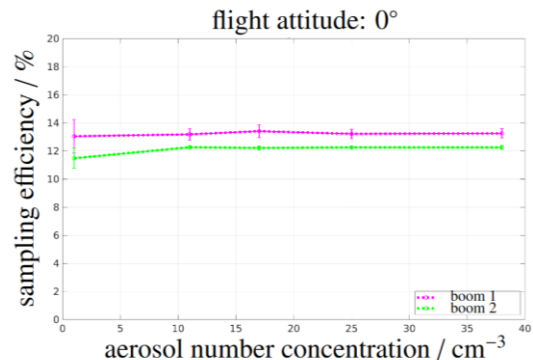


Figure 11: Sampling efficiency  $\eta$  related to initial aerosol number concentrations (ranging from 1 to  $38 \text{ cm}^{-3}$ ) for the angle of attack of  $0^\circ$ .

In the following, the upright boom is denoted by 1 and the downside-oriented boom as 2. Figure 10 shows the number of impacted particles as a function of aerosol number concentrations, for the  $0^\circ$  angle of

attack. Vertical bars represent the dispersion of simulated impactions obtained from four independent simulation runs. The results show that the number of impacted aerosols almost linearly increases with increasing aerosol number concentration. However, the number of particles collected as a function of the initial number concentration increases differently for each of the collection surfaces attached to boom 1 or 2. To determine the sampling efficiencies,  $\eta$  normalized to the cross-sectional area of the collectors is calculated as follows:

$$\eta = \frac{C_{impaction}}{C_{released}} \cdot \frac{A_{inlet}}{A_{impaction}}, \quad (10)$$

where  $C_{impaction}$  is the number of impacted particles (presented in *Figure 9*),  $C_{released}$  the number of released particles,  $A_{inlet}$  the surface of the particle inlet, and  $A_{impaction}$  the cross-section area of the collector. For the angle of attack of  $0^\circ$  (*Figure 11*), the sampling efficiencies are 13% (boom 1) and 12% (boom 2). The marginal difference of 1% in the collection efficiency of the two individually oriented collection surfaces can be explained by the asymmetric instrument assemblies at the tip of the instrument module (upstream of the particle collection position), which may have different effects on particle impactions. Similarly, the efficiency for different angles of attack (cf. *Figure 8*) can be investigated in the future.

### Summary and Conclusion

Simulated flow fields around the instrument module of a rocket-borne payload at supersonic speeds and different angles of attack with COMSOL®'s High Mach Number Continuum Flow Interface, provided by the COMSOL® CFD Module, support the development of an impaction-based, free-stream particle collector for nanometer-sized aerosols. To this end, the simulated flow fields were analyzed with their flow field variables and in terms of the evolving boundary layer around the instrument module. The particle trajectory simulations reveal the effectiveness of the developed aerodynamic design and arrangement of the probe collector under mesospheric conditions. The collector surfaces are located within the free flow (well outside the boundary layer), mostly unaffected by the evolving shockwave, and the design of the collector surfaces in a non-aerodynamic shape favors aerosol collection. Due to the radial arrangement of the booms with attached collectors around the instrument module, at least two of the collector surfaces are permanently exposed to the airflow during the collection phase, regardless of the angles of attack of  $0^\circ$  and  $\pm 30^\circ$ . Finally, the collection efficiency was simulated as a function of the initial particle number concentration, and it was found that the collection position in the wake of asymmetric fore built structures could play a role, albeit a minor one. In the future, the influence on the impaction

efficiencies of varying angles of attack can be investigated. The simulation results raise confidence that effective particle collection in the free stream at supersonic air speeds is feasible on designed collector surfaces in the elaborated configuration. However, the main challenge remains to keep the collector surfaces absolutely free of contamination prior to and after exposure so as not to entirely obscure the sample which was taken in the measurement region. Ultimately, the factual rocket flight is pending, which alone could complete the proof of concept of this development and also serve to validate (or adjust, if necessary) our COMSOL® model based on real observations. A successful in-flight particle collection and an analyzable sample have great potential to provide crucial insights into understanding NLC formation processes that were previously unavailable.

### References

- [1] J. Plane, "Cosmic dust in the earth's atmosphere.," *Chemical Society Reviews*, vol. 41, p. 6507–6518, 2012.
- [2] J. Plane, "Atmospheric chemistry of meteoric metals.," *Chemical reviews*, vol. 103, p. 4963–4984, 2003.
- [3] L. Megner, M. Rapp and J. Gumbel, "Distribution of meteoric smoke–sensitivity to microphysical properties and atmospheric conditions," *Atmospheric Chemistry and Physics*, vol. 6, p. 4415–4426, 2006.
- [4] R. Saunders, S. Dhomse, W. Tian, M. C. Chipperfield and .. Plane, "Interactions of meteoric smoke particles with sulphuric acid in the Earth's stratosphere," *Atmospheric chemistry and physics*, vol. 12, p. 4387–4398, 2012.
- [5] J. Plane, W. Feng and E. Dawkins, "The mesosphere and metals: Chemistry and changes," *Chemical reviews*, vol. 115, p. 4497–4541, 2015.
- [6] H. Wilms, M. Rapp and A. Kirsch, "Nucleation of mesospheric cloud particles: Sensitivities and limits," *Journal of Geophysical Research: Space Physics*, vol. 121, p. 2621–2644, 2016.
- [7] V. L. Frankland, A. James, J. Carrillo-Sánchez, D. Nesvorný, P. and P. J. P., "CO oxidation and O2 removal on meteoric material in Venus' atmosphere," *Icarus*, vol. 296, p. 150–162, 2017.
- [8] A. James, J. Brooke, T. Mangan, T. Whale, J. Plane and B. Murray, "Nucleation of nitric acid hydrates in polar stratospheric clouds by meteoric material," *Atmospheric Chemistry and Physics*, vol. 18, p. 4519–4531, 2018.
- [9] R. Turco, O. Toon, R. Whitten, R. Keesee and D. Hollenbach, "Noctilucent clouds: Simulation studies of their genesis, properties and global influences," *Planetary and Space Science*, vol. 30, p. 1147–1181, 1982.
- [10] M. Rapp and G. Thomas, "Modeling the microphysics of mesospheric ice particles: Assessment of current capabilities and basic sensitivities," *Journal of Atmospheric and Solar-Terrestrial Physics*, vol. 68, p. 715–744, 2006.
- [11] G. Baumgarten and J. Fiedler, "Vertical structure of particle properties and water content in noctilucent clouds," *Geophysical research letters*, vol. 35, 2008.
- [12] M. Hervig, M. Rapp, R. Latteck and L. Gordley, "Observations of mesospheric ice particles from the ALWIN radar and SOFIE," *Journal of Atmospheric and Solar-Terrestrial Physics*, vol. 73, p. 2176–2183, 2011.

- [13] M. Rapp and F. Lübken, "Polar mesosphere summer echoes (PMSE): Review of observations and current understanding," *Atmospheric chemistry and physics*, vol. 4, p. 2601–2633, 2004.
- [14] H. Asmus, H. Wilms, B. Strelnikov and M. Rapp, "On the heterogeneous nucleation of mesospheric ice on meteoric smoke particles: Microphysical modeling," *Journal of Atmospheric and Solar-Terrestrial Physics*, vol. 118, p. 180–189, 2014.
- [15] COMSOL Multiphysics®, "COMSOL AB, Stockholm, Sweden. Version 5.6. URL: www.comsol.com," 2020.
- [16] W. Tozer and D. Beeson, "Optical model of noctilucent clouds based on polarimetric measurements from two sounding rocket campaigns," *Journal of Geophysical Research*, vol. 79, p. 5607–5612, 1974.
- [17] G. Thomas, "Mesospheric clouds and the physics of the mesopause region," *Reviews of Geophysics*, vol. 29, p. 553–575, 1991.
- [18] F. Lübken, "Eisteilchen in 80–90 km Höhe: Indikatoren für die niedrigsten Temperaturen in der Erdatmosphäre," *Promet*, vol. 31, p. 19–24, 2005.
- [19] M. Hervig, L. Gordley, L. Deaver, D. Siskind, M. Stevens, R. I. J.M., S. Bailey, L. Megner and C. Bardeen, "First satellite observations of meteoric smoke in the middle atmosphere," *Geophysical Research Letters*, vol. 36, 2009.
- [20] M. Horányi, J. Gumbel, G. Witt and S. Robertson, "Simulation of rocket-borne particle measurements in the mesosphere.," *Geophysical research letters*, vol. 26, p. 1537–1540, 1999.
- [21] I. Strelnikova, M. R. S. Rapp and M. Sulzer, "Meteor smoke particle properties derived from Arecibo incoherent scatter radar observations.," *Geophysical Research Letters*, vol. 34, 2007.
- [22] M. Rapp, I. Strelnikova, B. Strelnikov, P. Hoffmann, M. Friedrich, J. Gumbel, L. Megner, U. Hoppe, S. Robertson and S. Knappmiller, "Rocket-borne in situ measurements of meteor smoke: Charging properties and implications for seasonal variation.," *Journal of Geophysical Research: Atmospheres*, vol. 115, 2010.
- [23] L. Lanci, B. Delmonte, D. Kent, V. Maggi, P. Biscaye and J. Petit, "Magnetization of polar ice: a measurement of terrestrial dust and extraterrestrial fallout," *Quaternary Science Reviews*, vol. 33, p. 20–31, 2012.
- [24] M. Rapp, J. Plane, B. Strelnikov, G. Stober, S. Ernst, J. Hedin, M. Friedrich and U. Hoppe, "In situ observations of meteor smoke particles (MSP) during the Geminids 2010: constraints on MSP size, work function and composition," *Annales geophysicae, Copernicus Publications Göttingen, Germany*, p. 1661–1673, 2012.
- [25] J. Hedin, F. Giovane, T. Waldemarsson, J. Gumbel, J. Blum, R. Stroud, L. Marlin, J. Moser, D. Siskind, K. Jansson, R. Saunders, M. Summersh, P. Reissaus, J. Stegman, J. Plane and M. Horányi, "The MAGIC meteoric smoke particle sampler," *Journal of Atmospheric and Solar-Terrestrial Physics*, vol. 118, p. 127–144, 2014.
- [26] K. Naumann, C. Kirchberger, O. Drescher, D. Hergarten, M. Zurkaulen, A. Haubl, S. Rest, H. Niedermaier and J. Ramsel, "Design of a hovering sounding rocket stage for measurements in the high atmosphere," 2020.
- [27] M. Baumgartner, R. Weigel, A. H. Harvey, F. Plöger, U. Achatz and P. Spichtinger, "Reappraising the appropriate calculation of a common meteorological quantity: potential temperature," *Atmos. Chem. Phys.*, vol. 20, p. 15585–15616, 2020.
- [28] F. Lübken, "Thermal structure of the Arctic summer mesosphere," *Journal of Geophysical Research: Atmospheres*, vol. 104, p. 9135–9149, 1999.
- [29] COMSOL Multiphysics®, "Introduction to the Particle Tracing Module," 2017.
- [30] G. Baumgarten, J. Fiedler, F. Lübken and G. Von Cossart, "Particle properties and water content of noctilucent clouds and their interannual variation," *Journal of Geophysical Research: Atmospheres*, vol. 113, 2008.
- [31] G. Von Cossart, J. Fiedler and U. Von Zahn, "Size distributions of NLC particles as determined from 3-color observations of NLC by ground-based lidar," *Geophysical Research Letters*, vol. 26, p. 1513–1516, 1999.
- [32] J. Hedin, J. Gumbel, T. Waldemarsson and F. Giovane, "The aerodynamics of the MAGIC meteoric smoke sampler," *Advances in Space Research*, vol. 40, p. 818–824, 2007.